

Black Holes with Multiple Photon Spheres

Guangzhou Guo^{a,*}, Yuhang Lu^{a,†}, Peng Wang^{a,‡}, Houwen Wu^{a,b,§} and Haitang Yang^{a,¶}

^a*Center for Theoretical Physics, College of Physics,
Sichuan University, Chengdu, 610064, China and*

^b*Department of Applied Mathematics and Theoretical Physics,
University of Cambridge, Wilberforce Road, Cambridge, CB3 0WA, UK*

Recently, asymptotically-flat black holes with multiple photon spheres have been discovered and found to produce distinctive observational signatures. In this paper, we focus on whether these black hole solutions are physically viable, e.g., satisfying energy conditions of interest. Intriguingly, black hole and naked singularity solutions with two photon spheres and one anti-photon sphere are shown to exist in physically reasonable models, which satisfy the null, weak, dominant and strong energy conditions. Our findings reveal that black holes with multiple photon spheres may not be frequent, but they are not exotic.

arXiv:2212.12901v3 [gr-qc] 5 Jan 2023

* gzguo@stu.scu.edu.cn

† luyuhang668@stu.scu.edu.cn

‡ pengw@scu.edu.cn

§ hw598@damtp.cam.ac.uk

¶ hyanga@scu.edu.cn

CONTENTS

I. Introduction	2
II. Energy Conditions	4
III. Double-Photon-Spheres Black Holes	5
A. Parametrized Black Holes	6
1. Perturbed Schwarzschild Black Holes	7
2. Johannsen-Psaltis Metric	8
3. New Parametrization	9
B. Specific Models	10
1. Einstein-Maxwell-Scalar Model	10
2. Black Holes in Galaxies	12
3. Hairy Schwarzschild Black Holes	13
IV. NLED Black Holes	14
A. Quasi-topological Electromagnetism	15
B. Born-Infeld Electrodynamics	16
C. Bardeen Metric	19
V. Conclusions	19
Acknowledgments	21
References	21

I. INTRODUCTION

The images of the supermassive black holes M87* [1–8] and Sgr A* [9–14] photographed by the Event Horizon Telescope collaboration and the gravitational waves from a binary black hole merger detected by LIGO and Virgo [15] will usher in a new era of black hole observations. For spherically symmetric black holes, photon spheres play a crucial role in imaging black holes, and generate the edge of black hole shadows. Moreover, photon spheres are closely related to quasinormal modes [16], whose superposition describes the ringdown stage of a binary black hole merger. Therefore, it is of great importance to investigate the role played by photon spheres in black hole observations.

Until recently, asymptotically-flat black holes were supposed to possess a single photon sphere outside the event horizon, particularly in a physically reasonable model. The single photon sphere would lead to a bright ring in black hole images and the absence of echoes in gravitational waveforms of ringdown signals. Intriguingly, the existence of two photon spheres outside the event horizon has been lately reported for dyonic black holes in Einstein's gravity where the quasi-topological electromagnetism is minimally coupled [17]. Later, it was found that the double-peak effective potential of scalar perturbations in the dyonic black holes with double photon spheres can give rise to echo signals [18].

Meanwhile, scalarized Reissner-Nordström (RN) black holes were constructed to understand the formation of hairy black holes [19], and we found that scalarized RN black holes can possess two photon spheres outside the event horizon in certain parameter regions [20]. Subsequently, optical appearances of accretion disks and luminous celestial spheres surrounding scalarized RN black holes were considered, which showed that an extra photon sphere can produce more bright rings in black hole images, noticeably increase the image flux and triple higher-order relativistic images [21, 22]. In addition, observational appearances of a star freely falling onto scalarized RN black holes have been numerically simulated, and it revealed that an extra photon sphere leads to a sharp peak of total luminosity and one more cascade of flashes seen by a specific observer [23].

On the other hand, the authors of [24] considered asymptotically-flat and spherically symmetric black hole solutions in various theories and found that there is only one photon sphere outside the event horizon if the Dominant Energy Condition (DEC) and Strong Energy Condition (SEC) are satisfied. This observation then led to the conjecture, which states that a violation of either SEC or DEC is a necessary condition for the existence of double photon spheres outside the event horizon. Additionally, it was proved in [24] that SEC requires a monotonically increasing $|g_{tt}|$ in Einstein's gravity. For dyonic black holes with double photon spheres, $|g_{tt}|$ was shown to have a wiggle outside the event horizon, and hence SEC is violated [17]. This discovery is consistent with the conjecture proposed in [24]. Although the existence of double photon sphere in black hole spacetime is new, it is well known that wormholes can have two photon spheres, one on each side of the wormholes. In Einstein's gravity, exotic matter is usually required to keep the mouths of traversable wormholes open, which may reinforce the conjecture.

Nevertheless, no fundamental principles prevent us from searching for black hole solutions with multiple photon spheres in a physically reasonable model, e.g., satisfying SEC and DEC. To this end, we investigate various parametrized black holes and specific models to discover solutions with double photon spheres and check energy conditions for them in this paper. The rest of the paper

is organized as follows. In Section II, we briefly review four energy conditions and a necessary condition for SEC. Black hole solutions with double photon spheres are considered in the context of parametrized black holes and specific black hole models in Section III. In Section IV, the existence of double photon spheres is discussed in the spacetime sourced by non-linear electromagnetic fields, where photons move along null geodesics of some effective metric. Finally, we conclude with a brief discussion in Section V. We set $16\pi G = 1$ throughout this paper.

II. ENERGY CONDITIONS

In this section, we briefly review energy conditions in general relativity and how the strong energy condition constrains black hole metric. The energy conditions are expected to impose restrictions on the stress-energy-momentum tensor $T_{\mu\nu}$ of matter fields in a physically reasonable model [25]. In particular, standard energy conditions for $T_{\mu\nu}$ in a D -dimensional spacetime are stated as follows:

- Null Energy Condition (NEC): $T_{\mu\nu}l^\mu l^\nu \geq 0$ for any null vector l^μ . It guarantees that the mass-energy density measured by an observer traversing any null orbit is non-negative.
- Weak Energy Condition (WEC): $T_{\mu\nu}v^\mu v^\nu \geq 0$ for any timelike vector v^μ . It guarantees that the mass-energy density measured by an observer traversing any timelike orbit is non-negative.
- DEC: $T_{\mu\nu}v^\mu v^\nu \geq 0$ and $J^\mu J_\mu \leq 0$ for any timelike vector v^μ , where $J^\mu \equiv T^\mu_\nu v^\nu$ is the energy flux measured by an observer with four-velocity v^μ . It guarantees that, for every timelike observer, the measured mass-energy is non-negative, and the total flux of energy momentum does not propagate faster than the speed of light.
- SEC: $\left(T_{\mu\nu} - \frac{Tg_{\mu\nu}}{D-2}\right)v^\mu v^\nu \geq 0$ for any timelike vector v^μ . It guarantees that timelike geodesic congruence locally converges, which implies that “gravity acts attractively” on matter moving along timelike geodesics.

In some orthonormal basis $\{e_a^\mu\}$ satisfying $e_a^\mu e_{b\mu} = \eta_{ab}$ and $g^{\mu\nu} = \eta^{ab}e_a^\mu e_b^\nu$, the components of the energy-momentum tensor in the orthonormal frame $T_{ab} = T_{\mu\nu}e_a^\mu e_b^\nu$ can be written as in a canonical form [26]. If the canonical form of T_{ab} is type I (i.e., $T_{ab} = \text{diag}(\rho, p_1, p_2, \dots, p_{D-1})$), the aforementioned energy conditions can be expressed as follows:

- NEC: $\rho + p_i \geq 0$ for $i = 1, 2, \dots, D - 1$.
- WEC: $\rho \geq 0$ and $\rho + p_i \geq 0$.
- DEC: $\rho \geq |p_i|$ for $i = 1, 2, \dots, D - 1$ and $\rho \geq 0$.
- SEC: $(D - 3)\rho + \sum_{i=1}^{D-1} p_i \geq 0$ and $\rho + p_i \geq 0$ for $i = 1, 2, \dots, D - 1$.

For a spherically symmetric and static black hole solution in general relativity

$$ds^2 = -f(r) dt^2 + \frac{dr^2}{h(r)} + R(r) (d\theta^2 + \sin^2 \theta d\varphi^2), \quad (1)$$

the Einstein field equations yield [24]

$$f'(r) > \frac{1}{R(r)} \sqrt{\frac{f(r)}{h(r)}} \int_{r_h}^r R(r') \sqrt{\frac{h(r')}{f(r')}} (\rho + p_1 + p_2 + p_3) dr'. \quad (2)$$

Here, r_h is the event horizon radius, and the orthonormal frame is chosen as the static frame,

$$e_0^\mu dx_\mu = \frac{dt}{\sqrt{f(r)}}, e_1^\mu dx_\mu = \sqrt{h(r)} dr, e_2^\mu dx_\mu = \frac{1}{\sqrt{R(r)}}, e_3^\mu dx_\mu = \frac{1}{\sqrt{R(r)} \sin \theta}. \quad (3)$$

Interestingly, eqn. (2) shows that $f'(r) > 0$ is a necessary condition for SEC. In other words, if SEC is respected, $f(r)$ must be monotonically increasing. From this property, it was conjectured in [24] that, for an asymptotically-flat black hole, “a violation of either the dominant or the strong energy condition is a necessary condition for the existence of an anti-photon sphere outside a regular black hole horizon.”

III. DOUBLE-PHOTON-SPHERES BLACK HOLES

For the black hole solution (1), the Lagrangian governing null geodesics is

$$\mathcal{L} = \frac{1}{2} \left[-f(r) \dot{t}^2 + \frac{\dot{r}^2}{h(r)} + R(r) (\dot{\theta}^2 + \sin^2 \theta \dot{\varphi}^2) \right], \quad (4)$$

where dots stand for derivative with respect to the affine parameter λ . Due to spherical symmetry, we can confine ourselves to null geodesics on the equatorial plane. Since t and φ do not explicitly appear in the Lagrangian, null geodesics can be characterized by the energy E and the angular momentum L ,

$$E = -p_t = f(r) \dot{t}, \quad L = p_\varphi = R(r) \dot{\varphi}. \quad (5)$$

Moreover, the condition $\mathcal{L} = 0$ gives the radial component of the null geodesic equations,

$$\frac{f(r)}{h(r)} \frac{\dot{r}^2}{L^2} + V_{\text{eff}}(r) = \frac{1}{b^2}, \quad (6)$$

where $b \equiv L/E$ is the impact parameter. Here, we define the effective potential for null geodesics,

$$V_{\text{eff}}(r) = \frac{f(r)}{R(r)}, \quad (7)$$

which does not depend on the rr-component of the metric.

A circular null geodesic occurs at an extremum of the effective potential $V_{\text{eff}}(r)$, and the radius r_c of the geodesic is determined by

$$V_{\text{eff}}(r_c) = b_c^{-2}, \quad V'_{\text{eff}}(r_c) = 0, \quad (8)$$

where b_c is the impact parameter of the geodesic. In addition, local maxima and minima of the effective potential correspond to unstable and stable circular null geodesics, respectively. The unstable and stable circular null geodesics would constitute a photon sphere and an anti-photon sphere, respectively. Moreover, an asymptotically-flat black hole has $V_{\text{eff}}(\infty) = 0 = V_{\text{eff}}(r_h)$ and $V_{\text{eff}}(r) > 0$ for $r > r_h$, which indicates that there must exist at least one photon sphere outside the event horizon, and the number of photon spheres is always one more than the number of anti-photon spheres. Note that the same result has been reported in [27–30]. Particularly, the existence of an anti-photon sphere means two photon spheres outside the event horizon. If a null stable circular geodesic is at $r = r_c$, the conditions $V'_{\text{eff}}(r_c) = 0$ and $V''_{\text{eff}}(r_c) > 0$ give $f''(r_c) > 0$. So a black hole with double photon spheres should have $f''(r) > 0$ at some point. It is worth noting that NEC has been shown to be satisfied at anti-photon spheres [31].

A. Parametrized Black Holes

In this subsection, we explore parameter regions of the existence of double photon spheres in some parametrized black hole metrics, which contain a set of parameters measuring deviations from the Schwarzschild metric. As previously stated, the effective potential $V_{\text{eff}}(r)$ and the necessary condition for SEC (i.e., $f'(r) > 0$) are independent of $h(r)$ while the validity of the energy conditions generally depends on $h(r)$. Therefore, we also investigate two kinds of parameter regions where $f'(r) > 0$ regardless of $h(r)$, and the energy conditions are satisfied assuming $f(r) = h(r)$, respectively.

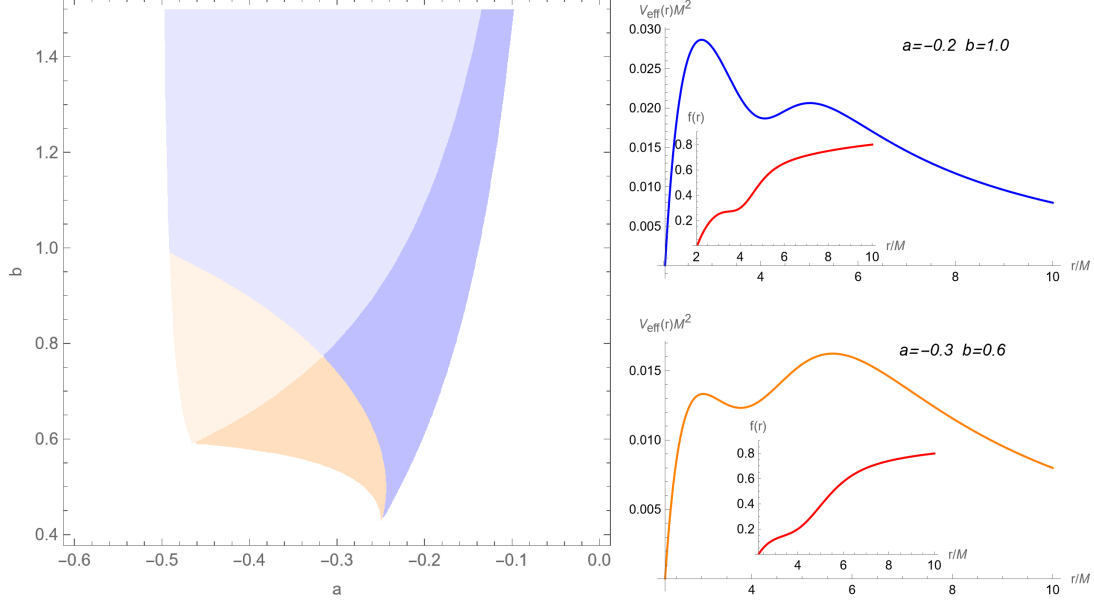


FIG. 1. For the perturbed Schwarzschild metric (9) with $r_0 = 4M$, there are two photon spheres outside the event horizon in the blue and orange regions of the left panel. In the blue/orange regions, the effective potential at the inner photon sphere is higher/lower than that at the outer one. In the dark blue and orange regions, the metric function $f(r)$ is monotonic, which is a necessary condition for SEC. The right panels show that the effective potential has a minimum, corresponding to an anti-photon sphere, near $r = 4M$.

1. Perturbed Schwarzschild Black Holes

Consider a small perturbation, which may be induced by environmental effects, to the Schwarzschild metric. Specifically, we model the perturbation by the Pöschl-Teller potential, and hence the perturbed Schwarzschild metric has

$$f(r) = 1 - \frac{2M}{r} + \frac{a}{\cosh^2[b(r - r_0)/M]}, \quad (9)$$

where the parameters a , b and r_0 describe the amplitude, the width and the location of the perturbation, respectively. In the left panel of FIG. 1, colored regions, where two photon spheres exist outside the event horizon, are displayed in the a - b parameter space with $r_0 = 4M$:

- Blue regions: The potential peak at the inner photon sphere is higher than that at the outer one. In this case, the two photon spheres can both play a role in determining optical appearances of luminous matters around black holes [20–22].
- Orange regions: The potential peak at the inner photon sphere is lower than that at the outer one. In this case, light rays in the vicinity of the inner photon sphere can not escape to

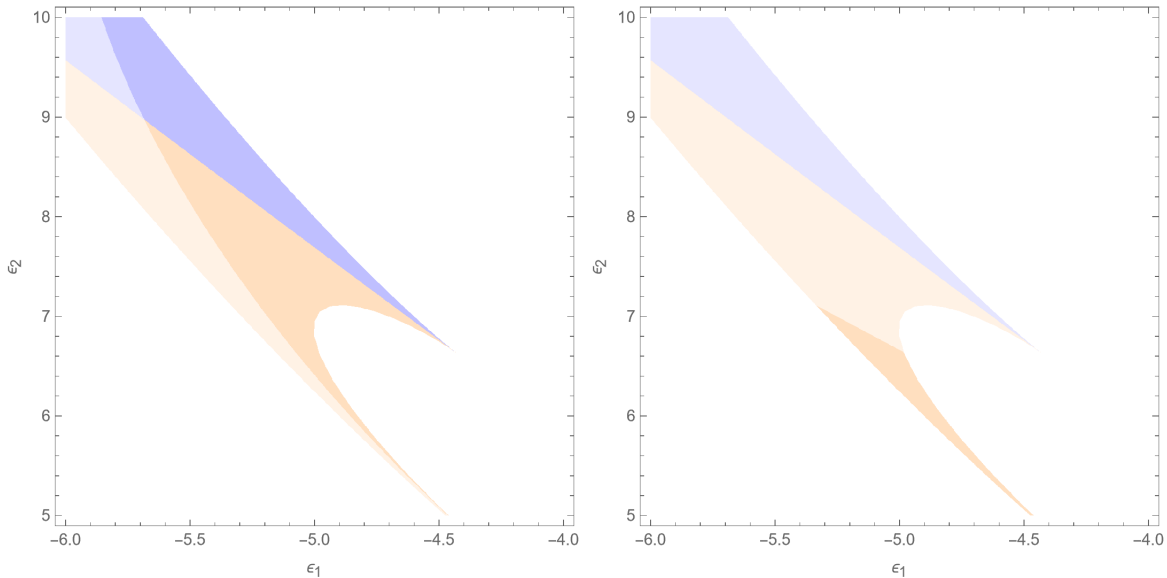


FIG. 2. For the JP metric (10) with $\epsilon_{k>2} = 0$, two photon spheres exist outside the event horizon in the blue and orange regions of the ϵ_1 - ϵ_2 parameter space. The inner potential peak is higher and lower than the outer one in the blue and orange regions, respectively. In the dark blue and orange regions, $f(r)$ is monotonic in the left panel, and NEC, WEC and DEC are respected in the right panel, where $f(r) = h(r)$ is assumed.

infinity, making this photon sphere invisible to distant observers. However, the inner photon sphere is closely related to long-lived quasinormal modes [32] and echo signals [33].

Moreover, $f(r)$ is a monotonically increasing function in the dark blue and orange regions of the left panel of FIG. 1. In addition, representative examples of the effective potential $V_{\text{eff}}(r)$ and the metric function $f(r)$ in the dark blue and orange regions are given in the upper-right and lower-right panels of FIG. 1, respectively. It shows that $f(r)$ is convex with $f''(r) > 0$ around $r = 4M$, where $V_{\text{eff}}(r)$ has a minimum. If one assumes $f(r) = h(r)$, the four energy conditions are found to be violated in the parameter space of FIG. 1.

2. Johannsen-Psaltis Metric

The metric function of the Johannsen-Psaltis (JP) metric can be written as [34, 35]

$$f(r) = \left(1 - \frac{2M}{r}\right) \left[1 + \sum_{k=1}^{\infty} \epsilon_k \left(\frac{M}{r}\right)^k\right], \quad (10)$$

where the coefficients ϵ_k are post-Newtonian-like parameters. In FIG. 2, we focus on the case with $\epsilon_{k>2} = 0$. Blue and orange regions in the ϵ_1 - ϵ_2 parameter space denote parameter regions

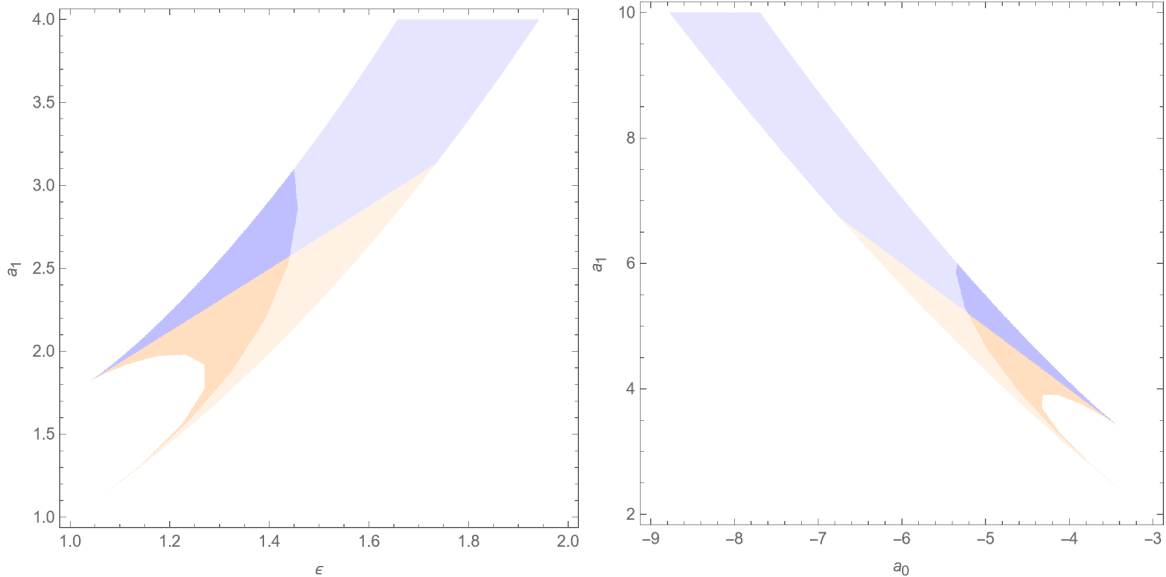


FIG. 3. For the new parametrization (11) with $a_{i>1} = 0$, two photon spheres exist in the blue and orange regions of the ϵ - a_1 parameter space with $a_0 = 0$ (**Left**) and the a_0 - a_1 parameter space with $\epsilon = 0$ (**Right**). The inner potential peak is higher and lower than the outer one in the blue and orange regions, respectively. In the dark blue and orange regions, $f(r)$ is monotonically increasing.

where two photon spheres exist. The inner potential peak is higher/lower than the outer one in the blue/orange regions. In the left panel, $f'(r) > 0$ in the dark orange and blue regions. In the case with $f(r) = h(r)$, the JP metric in the dark orange region of the right panel satisfies NEC, WEC and DEC. However, SEC is always violated in the colored regions.

3. New Parametrization

To better reproduce deviations from the Schwarzschild metric in the strong-field regime, a new parametrization for spherically symmetric black holes has been proposed [36–38],

$$f(r) = \left(1 - \frac{r_0}{r}\right) \left[1 - \epsilon \frac{r_0}{r} + (a_0 - \epsilon) \frac{r_0^2}{r^2} + \tilde{A} \left(1 - \frac{r_0}{r}\right) \frac{r_0^3}{r^3}\right], \quad (11)$$

where r_0 is the horizon radius, and

$$\tilde{A}(x) = \frac{a_1}{1 + \frac{a_2 x}{1 + \frac{a_3 x}{1 + \dots}}}. \quad (12)$$

The parameters ϵ , a_0 and a_i are used to characterize the black hole metric. Current observational constraints on the PPN parameters imply $a_0 \sim 10^{-4}$ [36]. For simplicity, we also set $a_{i>1} = 0$. In FIG. 3, we consider two cases with $a_0 = 0$ and $\epsilon = 0$ in the left and right panels, respectively.

Two photon spheres exist outside the event horizon in the blue and orange regions, and the inner potential peak is higher and lower than the outer one in the blue and orange regions, respectively. In addition, $f(r)$ is monotonically increasing in the dark blue and orange regions. The energy conditions are checked for the colored regions assuming $f(r) = h(r)$, and it is found that only NEC and WEC are respected in the small lower-left tip of the orange region in the left panel.

B. Specific Models

1. Einstein-Maxwell-Scalar Model

Recently, a novel class of Einstein-Maxwell-scalar (EMS) models have been proposed to study the spontaneous scalarization of RN black holes [19, 39–42]. In such models, the scalar field can trigger a tachyonic instability to form spontaneously scalarized hairy black holes from RN black holes. The action of the EMS model is

$$S = \int d^4x \sqrt{-g} \left[\mathcal{R} - 2\partial_\mu \phi \partial^\mu \phi - e^{\alpha\phi^2} F_{\mu\nu} F^{\mu\nu} \right], \quad (13)$$

where \mathcal{R} is the Ricci scalar, the scalar field ϕ is non-minimally coupled to the electromagnetic field A_μ with the coupling function $e^{\alpha\phi^2}$, and $F_{\mu\nu} = \partial_\mu A_\nu - \partial_\nu A_\mu$ is the electromagnetic field strength tensor. Restricting to static and spherically symmetric black hole solutions, one can have the generic ansatz

$$ds^2 = -N(r)e^{-2\delta(r)} dt^2 + \frac{1}{N(r)} dr^2 + r^2 (d\theta^2 + \sin^2 \theta d\varphi^2),$$

$$A_\mu dx^\mu = V(r)dt \text{ and } \phi = \phi(r). \quad (14)$$

In the static orthonormal basis, we find

$$\begin{aligned} T_{00} &= 2N(r) [\phi'(r)]^2 + 2e^{2\delta(r)+\alpha\phi^2(r)} [V'(r)]^2 = \rho, \\ T_{11} &= 2N(r) [\phi'(r)]^2 - 2e^{2\delta(r)+\alpha\phi^2(r)} [V'(r)]^2 = p_1, \\ T_{22} &= -2N(r) [\phi'(r)]^2 + 2e^{2\delta(r)+\alpha\phi^2(r)} [V'(r)]^2 = p_2, \\ T_{33} &= -2N(r) [\phi'(r)]^2 + 2e^{2\delta(r)+\alpha\phi^2(r)} [V'(r)]^2 = p_3. \end{aligned} \quad (15)$$

Using the aforementioned criteria for the energy conditions, it is easily found that NEC, WEC, DEC and SEC are all satisfied for the black hole solution (14) in the EMS model.

To obtain the black hole solution (14), one needs to impose proper boundary conditions at the

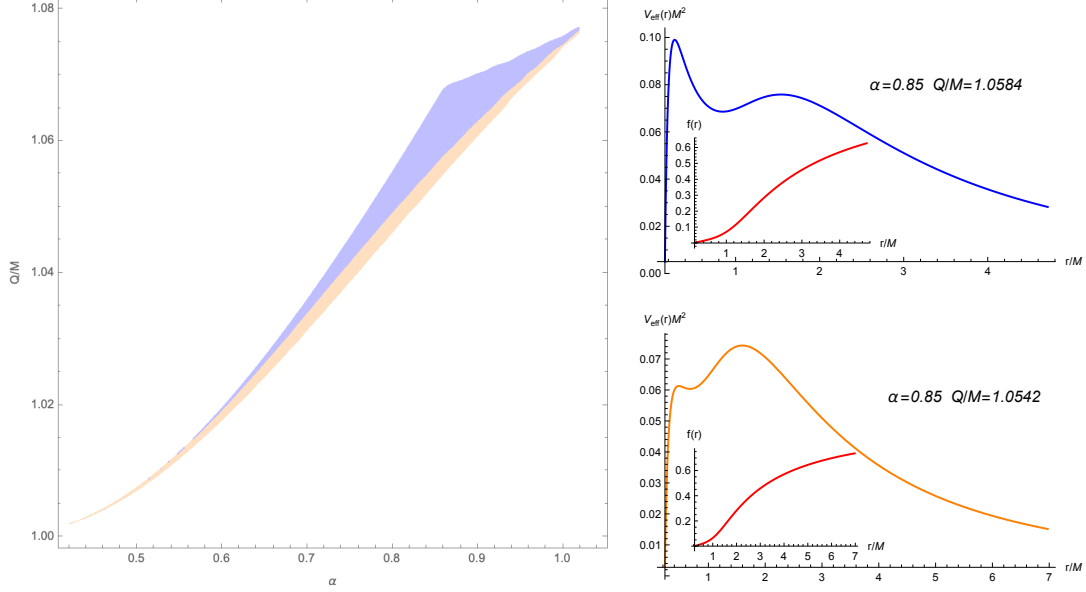


FIG. 4. **Left:** The parameter regions of scalarized RN black hole (18) that double photon spheres exist. In the blue/orange region, the effective potential at the inner photon sphere is higher/lower than that at the outer one. As discussed in the text, NEC, WEC, DEC and SEC are always satisfied. **Right:** The metric function $f(r) = N(r)e^{-2\delta(r)}$ and the effective potential $V_{eff}(r)$ of representative black holes in the blue and orange regions are presented in the upper and lower panels, respectively. It shows that $f(r)$ is monotonically increasing, which is a necessary condition for the validity of SEC.

event horizon r_h and spatial infinity,

$$\begin{aligned}
 N(r_h) &= 0, \quad \delta(r_h) = \delta_0, \quad \phi(r_h) = \phi_0, \quad V(r_h) = 0, \\
 N(\infty) &= 1, \quad \delta(\infty) = 0, \quad \phi(\infty) = 0, \quad V(\infty) = \Phi,
 \end{aligned}
 \tag{16}$$

where δ_0 and ϕ_0 can be used to characterize black hole solutions, and Φ is the electrostatic potential. Specifically, $\phi_0 = \delta_0 = 0$ correspond to the scalar-free solutions with $\phi = 0$, i.e., RN black holes. When non-zero values of ϕ_0 and δ_0 are admitted, scalarized RN black holes with a non-trivial scalar field ϕ can be obtained by a shooting method.

In the left panel of FIG. 4, we display blue and orange regions in the α - Q/M parameter space, in which double photon spheres exist outside the event horizon. Here, the parameters M and Q are the black hole mass and charge, respectively. In the blue/orange region, the potential peak at the inner/outer photon sphere is higher than that at the outer/inner photon sphere. The right panels of FIG. 4 present the metric function $f(r) = N(r)e^{-2\delta(r)}$ and the effective potential $V_{eff}(r)$ for black holes in the blue and orange regions. As expected, $f(r)$ is shown to monotonically increase, which is required by the validity of SEC.

2. Black Holes in Galaxies

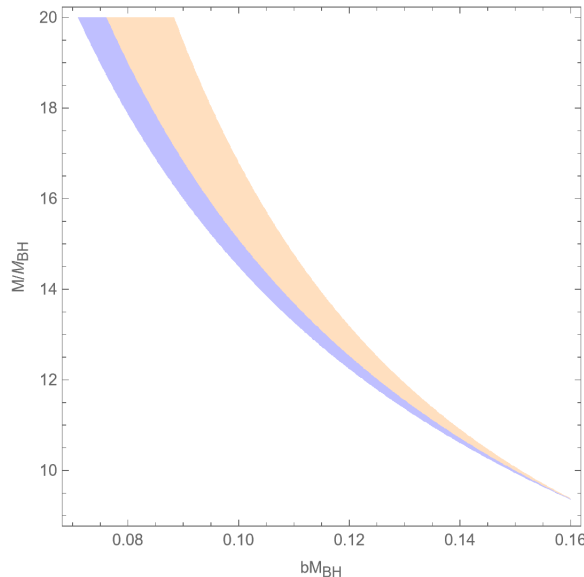


FIG. 5. For the metric describing black holes in galaxies (17), two photon spheres exist in the blue and orange regions of the $bM_{\text{BH}}-M/M_{\text{BH}}$ parameter space. The inner potential peak is higher than the outer one in the blue region, while the outer potential peak is higher than the inner one in the orange region.

To describe the geometry of supermassive black holes residing in galaxies, a family of solutions of Einstein's gravity has been constructed by minimally coupling the gravity sector to an anisotropic fluid [43]. In particular, the geometry can be written as

$$\begin{aligned}
 ds^2 &= - \left(1 - \frac{2M_{\text{BH}}}{r} \right) e^{\Upsilon} dt^2 + \frac{dr^2}{1 - 2m(r)/r} + r^2 d\Omega^2, \\
 \Upsilon &= -\pi \sqrt{\frac{M}{\xi}} + 2 \sqrt{\frac{M}{\xi}} \arctan \frac{r + b^{-1} - M}{\sqrt{M\xi}}, \\
 \xi &= 2b^{-1} - M + 4M_{\text{BH}}, \\
 m(r) &= M_{\text{BH}} + \frac{Mr^2}{(b^{-1} + r)^2} \left(1 - \frac{2M_{\text{BH}}}{r} \right)^2,
 \end{aligned} \tag{17}$$

where M_{BH} is the black hole mass, and M and b^{-1} are the total mass and the typical lengthscale of the halo surrounding the black hole. When $M \rightarrow 0$ and $b \rightarrow 0$, the above metric reduces to the Schwarzschild metric. Moreover, it showed that the anisotropic fluid satisfies NEC, WEC and SEC, and DEC is only violated close to the event horizon. Nevertheless, the anisotropic fluid has arbitrarily small pressure and density near the horizon, and hence the violation of DEC may play no role in the spacetime dynamics [43]. In FIG. 5, we present blue and orange regions in the $bM_{\text{BH}}-M/M_{\text{BH}}$ parameter space, which admit the black hole solutions with double photon spheres.

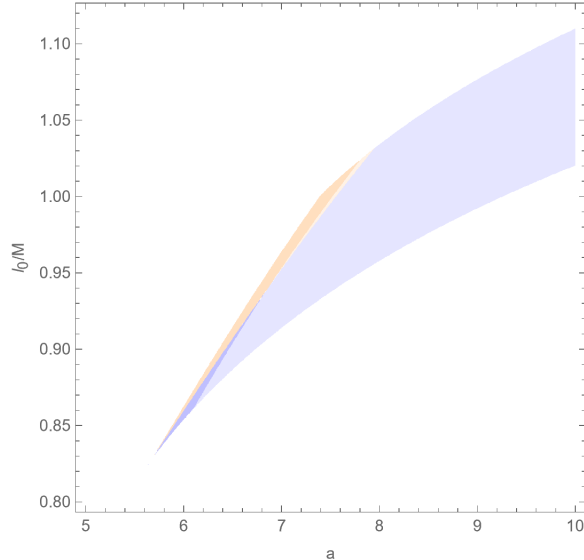


FIG. 6. The parameter region of hairy Schwarzschild black holes (18) that double photon spheres exist. NEC and WEC are respected in the dark blue and orange regions. The inner potential peak is higher and lower than the outer one in the blue and orange regions, respectively.

In the blue/orange region, the potential peak at the inner/outer photon sphere is higher than that at the outer/inner photon sphere.

3. Hairy Schwarzschild Black Holes

In [44–46], a hairy black hole solution was obtained from the seed Schwarzschild vacuum by the gravitational decoupling approach. The metric of the hairy black hole is

$$ds^2 = - \left[1 - \frac{2M}{r} + ae^{-r/(M-l_0/2)} \right] dt^2 + \frac{dr^2}{1 - \frac{2M}{r} + ae^{-r/(M-l_0/2)}} + r^2 (d\theta^2 + \sin^2 \theta d\varphi^2), \quad (18)$$

where M is the black hole mass, a is the deviation parameter, and $l_0 < 2M$. When $a \rightarrow 0$, this metric reduces to the Schwarzschild metric. Moreover, the effective density and radial pressure are

$$\rho = -p_1 = \frac{ae^{-r/(M-l_0/2)}}{(M-l_0/2)r^2} (r - M + l_0/2), \quad (19)$$

and the effective tangential pressures are

$$p_2 = p_3 = \frac{ae^{-r/(M-l_0/2)}}{2(M-l_0/2)^2 r} (r - 2M + l_0). \quad (20)$$

In the left panel of FIG. 6, we display colored regions in the $a-l_0/M$ parameter space, which admit the black hole solutions with double photon spheres. In the blue/orange regions, the potential peak at the inner/outer photon sphere is higher than that at the outer/inner photon sphere.

Moreover, we also check whether the black hole solutions satisfy the energy conditions. It is found that DEC and SEC are always violated. Nevertheless, NEC and WEC can be respected in dark blue and orange regions in FIG. 6. From eqns. (19) and (20), the violations of NEC, WEC and SEC occur near the event horizon.

IV. NLED BLACK HOLES

If quantum corrections are considered, non-linear terms are usually added to the Maxwell Lagrangian, which gives rise to an effective model, namely non-linear electrodynamics (NLED). In the Einstein-NLED theory, various charged black hole solutions were investigated [47–53]. Due to self-interactions, photons usually do not propagate along null geodesics of the underlying black hole spacetime. Instead, they move along null geodesics of some effective geometry [54]. Therefore, we investigate the existence of double photon spheres in the effective metric of NLED black holes in this section.

Consider a (3 + 1) dimensional model of gravity coupled to a non-linear electromagnetic field A_μ ,

$$\mathcal{S} = \int d^4x \sqrt{-g} [R + 4\mathcal{L}(s, p)], \quad (21)$$

where $\mathcal{L}(s, p)$ is a general NLED Lagrangian. Here, s and p are two independent nontrivial scalars built from the field strength tensor $F_{\mu\nu} = \partial_\mu A_\nu - \partial_\nu A_\mu$ and none of its derivatives,

$$s = -\frac{1}{4}F^{\mu\nu}F_{\mu\nu} \text{ and } p = -\frac{1}{8}\epsilon^{\mu\nu\rho\sigma}F_{\mu\nu}F_{\rho\sigma}, \quad (22)$$

where $\epsilon^{\mu\nu\rho\sigma} \equiv -[\mu \nu \rho \sigma]/\sqrt{-g}$ is a totally antisymmetric Lorentz tensor, and $[\mu \nu \rho \sigma]$ is the permutation symbol. Varying the action (21) in terms of $g_{\mu\nu}$ and A_μ leads to equations of motion,

$$\begin{aligned} R_{\mu\nu} - \frac{1}{2}Rg_{\mu\nu} &= \frac{T_{\mu\nu}}{2}, \\ \nabla_\mu \left[\frac{\partial\mathcal{L}(s, p)}{\partial s} F^{\mu\nu} + \frac{1}{2} \frac{\partial\mathcal{L}(s, p)}{\partial p} \epsilon^{\mu\nu\rho\sigma} F_{\rho\sigma} \right] &= 0, \end{aligned} \quad (23)$$

where $T_{\mu\nu}$ is the energy-momentum tensor for the NLED field,

$$T_{\mu\nu} = 4g_{\mu\nu} \left[\mathcal{L}(s, p) - p \frac{\partial\mathcal{L}(s, p)}{\partial p} \right] + \frac{\partial\mathcal{L}(s, p)}{\partial s} F_\mu{}^\rho F_{\nu\rho}. \quad (24)$$

Here, we focus on the spherically symmetric and static black hole solution,

$$\begin{aligned} ds^2 &= -f(r) dt^2 + \frac{dr^2}{f(r)} + r^2 (d\theta^2 + \sin^2\theta d\varphi^2), \\ A &= A_t(r) dt - P \cos\theta d\varphi, \end{aligned} \quad (25)$$

where P is the black hole magnetic charge. Plugging the ansatz (25) into eqn. (23) yields

$$f(r) = 1 - \frac{2M}{r} - \frac{2}{r} \int_r^\infty r'^2 \left[\mathcal{L}(s, p) - A'_t(r) \frac{Q}{r^2} \right] dr, \quad (26)$$

where $A'_t(r)$ is determined by

$$\frac{\partial \mathcal{L}(s, p)}{\partial s} A'_t(r) - \frac{\partial \mathcal{L}(s, p)}{\partial p} \frac{P}{r^2} = \frac{Q}{r^2} \text{ with } s = \frac{A'_t(r) - P^2/r^4}{2} \text{ and } p = -\frac{A'_t(r) P}{r^2}. \quad (27)$$

Here, M and Q are the black hole mass and electrical charge, respectively. In the static orthonormal basis, the energy density and the pressures are

$$\begin{aligned} \rho = -p_1 &= \frac{2QA'_t(r)}{r^2} - 2\mathcal{L}(s, p), \\ p_2 = p_3 &= 2\mathcal{L}(s, p) + \frac{2A'_t(r) P}{r^2} \frac{\partial \mathcal{L}(s, p)}{\partial p} + \frac{2P^2}{r^4} \frac{\partial \mathcal{L}(s, p)}{\partial s}. \end{aligned} \quad (28)$$

In [54], characteristic equations of NLED fields were used to derive the effective geometry of photons in the underlying NLED black hole spacetime. If the NLED Lagrangian $\mathcal{L}_{\text{NLED}}$ is a function of s , i.e., $\mathcal{L}_{\text{NLED}} = \mathcal{L}(s)$, the effective metric is

$$g_{\text{eff}}^{\mu\nu} = -4 \frac{\partial \mathcal{L}(s)}{\partial s} g^{\mu\nu} - 64 \frac{\partial^2 \mathcal{L}(s)}{\partial s^2} F^\mu_\alpha F^{\alpha\nu}. \quad (29)$$

For $\mathcal{L}_{\text{NLED}} = \mathcal{L}(s, p)$, the full expression of $g_{\text{eff}}^{\mu\nu}$ is too lengthy to be included here. We refer readers to [54] for the expression of $g_{\text{eff}}^{\mu\nu}$. In the NLED black hole (25), the effective metric is spherically symmetric,

$$ds^2 = g_{\text{eff}}^{\mu\nu} dx_\mu dx_\nu = -f_{\text{eff}}(r) dt^2 + \frac{dr^2}{h_{\text{eff}}(r)} + R_{\text{eff}}(r) (d\theta^2 + \sin^2 \theta d\varphi^2), \quad (30)$$

which gives the effective potential of photons in the effective metric,

$$V_{\text{eff}}(r) = \frac{f_{\text{eff}}(r)}{R_{\text{eff}}(r)}. \quad (31)$$

A. Quasi-topological Electromagnetism

In [17], the squared norm of the topological 4-form $F \wedge F$ is added to the Maxwell theory, leading to the Quasi-topological Electromagnetism (QE). In particular, the electrodynamics Lagrangian is

$$\mathcal{L}(s, p) = s - aU^{(2)} = s + 8ap^2, \quad (32)$$

where $U^{(2)} = -\epsilon^{\nu_1\nu_2\nu_3\nu_4} \epsilon_{\mu_1\mu_2\mu_3\mu_4} F^{\mu_1\mu_2} F^{\mu_3\mu_4} F_{\nu_1\nu_2} F_{\nu_3\nu_4} / 8$ is the squared norm of the topological structure $F \wedge F$. Using eqn. (26), one can obtain the the metric function $f(r)$,

$$f(r) = 1 - \frac{2M}{r} + \frac{P^2}{r^2} + \frac{Q^2}{r^2} {}_2F_1 \left(\frac{1}{4}, 1, \frac{5}{4}; -\frac{16aP^2}{r^4} \right), \quad (33)$$

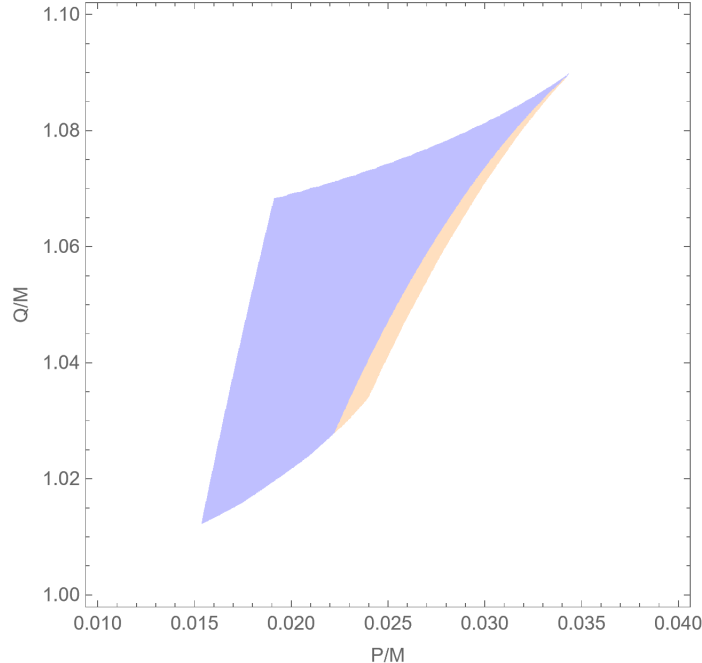


FIG. 7. For the dyonic black holes with a quasi-topological electromagnetic term (33), two photon spheres exist in the blue and orange regions of the P/M - Q/M parameter space with $a = 123.892$. The inner potential peak is higher and lower than the outer one in the blue and orange regions, respectively.

where ${}_2F_1(a, b, c; x)$ is the hypergeometric function. Moreover, the energy density and the pressures are

$$\begin{aligned} \rho = -p_1 &= \frac{2P^2}{r^4} + \frac{2Q^2}{16aP^2 + r^4}, \\ p_2 = p_3 &= \rho - \frac{64aP^2Q^2}{(16aP^2 + r^4)^2}, \end{aligned} \quad (34)$$

which shows that NEC, WEC and DEC are always satisfied. Nevertheless, SEC is not necessarily satisfied.

Since $\partial^2 \mathcal{L}(s, p) / \partial s^2 = 0 = \partial^2 \mathcal{L}(s, p) / \partial s \partial p$ in the QE, the effective metric of photons is just the underlying spacetime (33). In other words, the non-linear term in the quasi-topological electromagnetism does not induce a modification on the spacetime metric for photons. In FIG. 7, we display colored regions, where the QE black holes have two photon spheres. Moreover, we find that SEC is always violated even though $f(r)$ can monotonically increase in some parameter region.

B. Born-Infeld Electrodynamics

The Born-Infeld (BI) electrodynamics was first proposed to smooth divergences of the electrostatic self-energy of point charges by introducing a cutoff on electric fields [55]. Later, it is realized

that BI electrodynamics can emerge from the low energy limit of string theory, which encodes the low-energy dynamics of D-branes. Coupling the BI electrodynamics field to gravity, the BI black hole solution was first obtained in [56, 57]. The BI electrodynamics is described by the Lagrangian density

$$\mathcal{L}(s, p) = \frac{1}{a} \left(1 - \sqrt{1 - 2as - a^2 p^2} \right), \quad (35)$$

where the coupling parameter a is related to the string tension α' as $a = (2\pi\alpha')^2$. Eqn. (26) gives

$$f(r) = 1 - \frac{2M}{r} - \frac{2(P^2 + Q^2)}{3\sqrt{r^4 + a(P^2 + Q^2)} + 3r^2} + \frac{4(P^2 + Q^2)}{3r^2} {}_2F_1\left(\frac{1}{4}, \frac{1}{2}, \frac{5}{4}; -\frac{a(P^2 + Q^2)}{r^4}\right). \quad (36)$$

The energy density and the pressures are

$$\begin{aligned} \rho = -p_1 &= \frac{4(P^2 + Q^2)}{r^2 \left[\sqrt{a(P^2 + Q^2) + r^4} + r^2 \right]}, \\ p_2 = p_3 &= \frac{4(P^2 + Q^2)}{\sqrt{a(P^2 + Q^2) + r^4} \left(\sqrt{a(P^2 + Q^2) + r^4} + r^2 \right)}, \end{aligned} \quad (37)$$

which indicate that NEC, WEC, DEC and SEC are always satisfied. Furthermore, the effective metric of photons is [58]

$$\begin{aligned} f_{\text{eff}}(r) &= h_{\text{eff}}^{-1}(r) = \frac{\sqrt{aP^2 + r^4}}{r^2} \left[\frac{aP^2 + r^4}{a(P^2 + Q^2) + r^4} \right]^{3/2} f(r), \\ R_{\text{eff}}(r) &= \frac{(aP^2 + r^4)^2}{r^4 \sqrt{a(P^2 + Q^2) + r^4}}. \end{aligned} \quad (38)$$

Depending on the values of the parameters a , M , P and Q , the metric function (36) can describe a naked singularity at $r = 0$ or a black hole. For the black hole solution with given a , P and Q , the horizon radius r_e and the mass M_e of extremal black holes are determined by $f(r_e) = 0 = d(rf(r))/dr|_{r=r_e}$, which gives

$$\begin{aligned} r_e &= \frac{\sqrt{4(P^2 + Q^2) - a}}{2}, \\ M_e &= \frac{\sqrt{4(P^2 + Q^2) - a}}{6} + \frac{8(P^2 + Q^2)}{6\sqrt{4(P^2 + Q^2) - a}} {}_2F_1\left(\frac{1}{4}, \frac{1}{2}, \frac{5}{4}; -\frac{16a(P^2 + Q^2)}{[4(P^2 + Q^2) - a]^2}\right). \end{aligned} \quad (39)$$

Moreover, the above equations show that extremal black holes do not exist if $a > 4(P^2 + Q^2)$. Therefore, when $a < 4(P^2 + Q^2)$ and $M > M_e$, the spacetime is a black hole. For $a > 4(P^2 + Q^2)$, one has $d(rf(r))/dr > 0$ and $\lim_{r \rightarrow 0} rf(r) = 4\Gamma\left(\frac{1}{4}\right)\Gamma\left(\frac{5}{4}\right)[a(P^2 + Q^2)]^{3/4}/(3a\sqrt{\pi}) - 2M$, which indicates that a naked singularity appears when

$$M < \frac{2\Gamma\left(\frac{1}{4}\right)\Gamma\left(\frac{5}{4}\right)[a(P^2 + Q^2)]^{3/4}}{3a\sqrt{\pi}}. \quad (40)$$

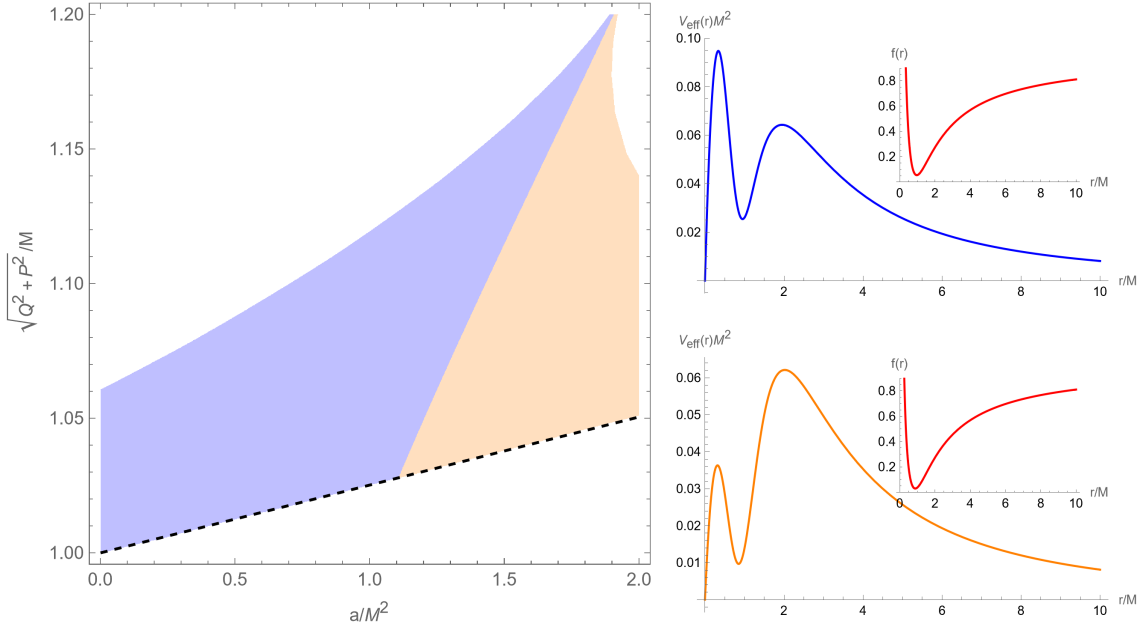


FIG. 8. **Left:** The Born-Infeld metric (36) above the dashed black line describes a naked singularity at $r = 0$. Naked singularity solutions in the blue and orange regions have two photon spheres. In the blue/orange regions, the effective potential at the inner photon sphere is higher/lower than that at the outer one. **Right:** The metric function $f(r)$ and the effective potential $V_{\text{eff}}(r)$ of representative naked singularity solutions in the blue and orange regions are displayed in the upper and lower panels, respectively.

In the left panel of FIG. 8, the dashed black line denotes the boundary between black hole and naked singularity solutions in the $a/M^2 - \sqrt{P^2 + Q^2}/M$ parameter space. Specifically, solutions above and below the dashed black line correspond to naked singularities and black holes, respectively.

For black hole solutions, we find that the effective potential V_{eff} of the effective metric (38) always has a single maximum outside the event horizon. Nevertheless, naked singularity solutions with the absence of the event horizon can possess two photon spheres and one anti-photon sphere in the effective metric. In the left panel of FIG. 8, the parameter regions where two photon spheres exist are presented in the $a/M^2 - \sqrt{P^2 + Q^2}/M$ parameter space. In the blue/orange region, the potential peak at the inner/outer photon sphere is higher than that at the outer/inner photon sphere. The panels in the right column offer representative examples in the blue and orange regions.

C. Bardeen Metric

To avoid singularities, Bardeen proposed a regular black hole model, which is described by the metric

$$f(r) = 1 - \frac{2Mr^2}{(r^2 + P^2)^{3/2}}. \quad (41)$$

Here, M is the mass of the Bardeen metric. In [59], it showed that P can be interpreted as the monopole charge of the magnetic field described by a NLED,

$$\mathcal{L}(s) = \frac{3M}{2P^3} \left(\frac{\sqrt{-2sP^2}}{1 + \sqrt{-2sP^2}} \right)^{5/2}. \quad (42)$$

Moreover, the Bardeen metric describes a regular black hole when $P \leq 4\sqrt{3}/9$. For $P > 4\sqrt{3}/9$, $f(r)$ is always positive, which indicates that the Bardeen metric represents a star with the absence of a singularity at $r = 0$. In addition, the energy density and the pressures are

$$\begin{aligned} \rho = -p_1 &= \frac{6MP^2}{(P^2 + r^2)^{5/2}}, \\ p_2 = p_3 &= -\rho + \frac{15MP^2r^2}{(P^2 + r^2)^{7/2}}, \end{aligned} \quad (43)$$

which indicates that NEC and WEC are satisfied. On the other hand, SEC and DEC are violated when r is small and large enough, respectively. Furthermore, the effective metric of photons is

$$\begin{aligned} f_{\text{eff}}(r) &= h_{\text{eff}}^{-1}(r) = \frac{16(r^2 + P^2)^{7/2}}{15r^6M} f(r), \\ R_{\text{eff}}(r) &= \frac{32(r^2 + P^2)^{9/2}}{15Mr^4(3r^2 - 4P^2)}. \end{aligned} \quad (44)$$

In the effective metric of regular Bardeen black holes (i.e., $P \leq 4\sqrt{3}/9$), there exists only one photon sphere outside the event horizon. On the other hand, when $4\sqrt{3}/9 < P < 0.781$, we find that the star solution can have two photon spheres, and the potential peak at the outer photon sphere is always higher than that at the inner photon sphere.

V. CONCLUSIONS

In this paper, we first explored the parameter space of parametrized black holes and some specific black hole models to find parameter regions where double photon spheres exist outside the event horizon. Moreover, the energy conditions, i.e., NEC, WEC, DEC and SEC, were considered for the black holes with double photon spheres. We then investigated the existence of double photon

spheres in the spacetime sourced by self-gravitating NLED fields, in which photons propagate along null geodesics of some effective metric. In summary, we found that

- Double photon spheres appear outside the event horizon in certain parameter regions of parametrized black holes. Moreover, $|g_{tt}|$ can monotonically increase outside the event horizon, which is required by SEC. When $g_{tt} = -g_{rr}^{-1}$, one or more energy conditions are violated, which implies that double-photon-spheres black holes satisfying the four energy conditions prefer $g_{tt}g_{rr} \neq -1$.
- In the EMS model satisfying the four energy conditions, scalarized RN black holes possess double photon spheres in some parameter regions, which provides a counterexample of the conjecture proposed in [24].
- Double photon spheres exist in naked singularity solutions sourced by BI electromagnetic fields, which satisfies the four energy conditions. In addition, the star solution of the Bardeen metric can have double photon spheres, in which NEC and WEC are respected.

Our findings suggest that multiple photon spheres can emerge in some parameter regions of black holes. Considering significant effects of extra photon spheres, it is highly desirable to check whether a given black hole solution can have multiple photon spheres outside the event horizon. If so, it is also important to obtain parameter regions where multiple photon spheres exist. To achieve this, we provide the *Mathematica* code, which can efficiently scan the black hole parameter space with the help of parallel computing to find multiple-photon-spheres parameter regions [60]. Moreover, the code can also give parameter regions where the energy conditions are satisfied by inputting the stress-energy tensor or simply the metric if Einstein's gravity is assumed. For NLED black holes, calculating the effective metric of NLED fields with $\mathcal{L}(s, p)$ is also included in the code. In this paper, we confined ourselves to Einstein's gravity. In future studies, looking for black holes with multiple photon spheres in modified gravity is of equivalent importance. We hope that the code can facilitate the search procedure.

Interestingly, the anti-photon sphere, which is composed of stable circular orbits and resides between two photon spheres, play a key role in the instability of black holes. In [32], some quasi-normal modes have been shown to be trapped around the anti-photon sphere for a long time. The long-lived modes may accumulate near the anti-photon sphere and eventually develop a non-linear instability, which could destabilize the background spacetime by the backreaction [61]. Recently, the authors of [62] used fully non-linear numerical evolutions to confirm that the anti-photon

sphere of ultracompact bosonic stars can trigger the instability. It is of great interest to study non-linear numerical evolutions of black holes with multiple photon spheres to address the non-linear instabilities of long-lived modes.

ACKNOWLEDGMENTS

We are grateful to Yiqian Chen and Qingyu Gan for useful discussions and valuable comments. This work is supported in part by NSFC (Grant No. 11875196, 11947225, 12105191, 12275183 and 12275184). Houwen Wu is supported by the International Visiting Program for Excellent Young Scholars of Sichuan University.

-
- [1] Kazunori Akiyama et al. First M87 Event Horizon Telescope Results. I. The Shadow of the Supermassive Black Hole. *Astrophys. J. Lett.*, 875:L1, 2019. [arXiv:1906.11238](https://arxiv.org/abs/1906.11238), [doi:10.3847/2041-8213/ab0ec7](https://doi.org/10.3847/2041-8213/ab0ec7). I
 - [2] Kazunori Akiyama et al. First M87 Event Horizon Telescope Results. II. Array and Instrumentation. *Astrophys. J. Lett.*, 875(1):L2, 2019. [arXiv:1906.11239](https://arxiv.org/abs/1906.11239), [doi:10.3847/2041-8213/ab0c96](https://doi.org/10.3847/2041-8213/ab0c96).
 - [3] Kazunori Akiyama et al. First M87 Event Horizon Telescope Results. III. Data Processing and Calibration. *Astrophys. J. Lett.*, 875(1):L3, 2019. [arXiv:1906.11240](https://arxiv.org/abs/1906.11240), [doi:10.3847/2041-8213/ab0c57](https://doi.org/10.3847/2041-8213/ab0c57).
 - [4] Kazunori Akiyama et al. First M87 Event Horizon Telescope Results. IV. Imaging the Central Supermassive Black Hole. *Astrophys. J. Lett.*, 875(1):L4, 2019. [arXiv:1906.11241](https://arxiv.org/abs/1906.11241), [doi:10.3847/2041-8213/ab0e85](https://doi.org/10.3847/2041-8213/ab0e85).
 - [5] Kazunori Akiyama et al. First M87 Event Horizon Telescope Results. V. Physical Origin of the Asymmetric Ring. *Astrophys. J. Lett.*, 875(1):L5, 2019. [arXiv:1906.11242](https://arxiv.org/abs/1906.11242), [doi:10.3847/2041-8213/ab0f43](https://doi.org/10.3847/2041-8213/ab0f43).
 - [6] Kazunori Akiyama et al. First M87 Event Horizon Telescope Results. VI. The Shadow and Mass of the Central Black Hole. *Astrophys. J. Lett.*, 875(1):L6, 2019. [arXiv:1906.11243](https://arxiv.org/abs/1906.11243), [doi:10.3847/2041-8213/ab1141](https://doi.org/10.3847/2041-8213/ab1141).
 - [7] Kazunori Akiyama et al. First M87 Event Horizon Telescope Results. VII. Polarization of the Ring. *Astrophys. J. Lett.*, 910(1):L12, 2021. [arXiv:2105.01169](https://arxiv.org/abs/2105.01169), [doi:10.3847/2041-8213/abe71d](https://doi.org/10.3847/2041-8213/abe71d).
 - [8] Kazunori Akiyama et al. First M87 Event Horizon Telescope Results. VIII. Magnetic Field Structure near The Event Horizon. *Astrophys. J. Lett.*, 910(1):L13, 2021. [arXiv:2105.01173](https://arxiv.org/abs/2105.01173), [doi:10.3847/2041-8213/abe4de](https://doi.org/10.3847/2041-8213/abe4de). I
 - [9] Kazunori Akiyama et al. First Sagittarius A* Event Horizon Telescope Results. I. The Shadow of the Supermassive Black Hole in the Center of the Milky Way. *Astrophys. J. Lett.*, 930(2):L12, 2022. [doi:10.3847/2041-8213/ac6674](https://doi.org/10.3847/2041-8213/ac6674). I

- [10] Kazunori Akiyama et al. First Sagittarius A* Event Horizon Telescope Results. II. EHT and Multiwavelength Observations, Data Processing, and Calibration. *Astrophys. J. Lett.*, 930(2):L13, 2022. [doi:10.3847/2041-8213/ac6675](https://doi.org/10.3847/2041-8213/ac6675).
- [11] Kazunori Akiyama et al. First Sagittarius A* Event Horizon Telescope Results. III. Imaging of the Galactic Center Supermassive Black Hole. *Astrophys. J. Lett.*, 930(2):L14, 2022. [doi:10.3847/2041-8213/ac6429](https://doi.org/10.3847/2041-8213/ac6429).
- [12] Kazunori Akiyama et al. First Sagittarius A* Event Horizon Telescope Results. IV. Variability, Morphology, and Black Hole Mass. *Astrophys. J. Lett.*, 930(2):L15, 2022. [doi:10.3847/2041-8213/ac6736](https://doi.org/10.3847/2041-8213/ac6736).
- [13] Kazunori Akiyama et al. First Sagittarius A* Event Horizon Telescope Results. V. Testing Astrophysical Models of the Galactic Center Black Hole. *Astrophys. J. Lett.*, 930(2):L16, 2022. [doi:10.3847/2041-8213/ac6672](https://doi.org/10.3847/2041-8213/ac6672).
- [14] Kazunori Akiyama et al. First Sagittarius A* Event Horizon Telescope Results. VI. Testing the Black Hole Metric. *Astrophys. J. Lett.*, 930(2):L17, 2022. [doi:10.3847/2041-8213/ac6756](https://doi.org/10.3847/2041-8213/ac6756). I
- [15] B.P. Abbott et al. Observation of Gravitational Waves from a Binary Black Hole Merger. *Phys. Rev. Lett.*, 116(6):061102, 2016. [arXiv:1602.03837](https://arxiv.org/abs/1602.03837), [doi:10.1103/PhysRevLett.116.061102](https://doi.org/10.1103/PhysRevLett.116.061102). I
- [16] Vitor Cardoso, Alex S. Miranda, Emanuele Berti, Helvi Witek, and Vilson T. Zanchin. Geodesic stability, Lyapunov exponents and quasinormal modes. *Phys. Rev. D*, 79:064016, 2009. [arXiv:0812.1806](https://arxiv.org/abs/0812.1806), [doi:10.1103/PhysRevD.79.064016](https://doi.org/10.1103/PhysRevD.79.064016). I
- [17] Hai-Shan Liu, Zhan-Feng Mai, Yue-Zhou Li, and H. Lü. Quasi-topological Electromagnetism: Dark Energy, Dyonic Black Holes, Stable Photon Spheres and Hidden Electromagnetic Duality. *Sci. China Phys. Mech. Astron.*, 63:240411, 2020. [arXiv:1907.10876](https://arxiv.org/abs/1907.10876), [doi:10.1007/s11433-019-1446-1](https://doi.org/10.1007/s11433-019-1446-1). I, IV A
- [18] Hyat Huang, Min-Yan Ou, Meng-Yun Lai, and H. Lu. Echoes from Classical Black Holes. 12 2021. [arXiv:2112.14780](https://arxiv.org/abs/2112.14780). I
- [19] Carlos A.R. Herdeiro, Eugen Radu, Nicolas Sanchis-Gual, and José A. Font. Spontaneous Scalarization of Charged Black Holes. *Phys. Rev. Lett.*, 121(10):101102, 2018. [arXiv:1806.05190](https://arxiv.org/abs/1806.05190), [doi:10.1103/PhysRevLett.121.101102](https://doi.org/10.1103/PhysRevLett.121.101102). I, III B 1
- [20] Qingyu Gan, Peng Wang, Houwen Wu, and Haitang Yang. Photon spheres and spherical accretion image of a hairy black hole. *Phys. Rev. D*, 104(2):024003, 2021. [arXiv:2104.08703](https://arxiv.org/abs/2104.08703), [doi:10.1103/PhysRevD.104.024003](https://doi.org/10.1103/PhysRevD.104.024003). I, III A 1
- [21] Qingyu Gan, Peng Wang, Houwen Wu, and Haitang Yang. Photon ring and observational appearance of a hairy black hole. *Phys. Rev. D*, 104(4):044049, 2021. [arXiv:2105.11770](https://arxiv.org/abs/2105.11770), [doi:10.1103/PhysRevD.104.044049](https://doi.org/10.1103/PhysRevD.104.044049). I
- [22] Guangzhou Guo, Xin Jiang, Peng Wang, and Houwen Wu. Gravitational Lensing by Black Holes with Multiple Photon Spheres. 4 2022. [arXiv:2204.13948](https://arxiv.org/abs/2204.13948). I, III A 1
- [23] Yiqian Chen, Guangzhou Guo, Peng Wang, Houwen Wu, and Haitang Yang. Appearance of an infalling star in black holes with multiple photon spheres. *Sci. China Phys. Mech. Astron.*, 65(12):120412, 2022.

- [arXiv:2206.13705](#), [doi:10.1007/s11433-022-1986-x](#). I
- [24] M. Cvetič, G. W. Gibbons, and C. N. Pope. Photon Spheres and Sonic Horizons in Black Holes from Supergravity and Other Theories. *Phys. Rev. D*, 94(10):106005, 2016. [arXiv:1608.02202](#), [doi:10.1103/PhysRevD.94.106005](#). I, II, II, V
- [25] Hideki Maeda and Cristian Martinez. Energy conditions in arbitrary dimensions. *PTEP*, 2020(4):043E02, 2020. [arXiv:1810.02487](#), [doi:10.1093/ptep/ptaa009](#). II
- [26] S. W. Hawking and G. F. R. Ellis. *The Large Scale Structure of Space-Time*. Cambridge Monographs on Mathematical Physics. Cambridge University Press, 2 2011. [doi:10.1017/CB09780511524646](#). II
- [27] Pedro V. P. Cunha and Carlos A. R. Herdeiro. Stationary black holes and light rings. *Phys. Rev. Lett.*, 124(18):181101, 2020. [arXiv:2003.06445](#), [doi:10.1103/PhysRevLett.124.181101](#). III
- [28] Shao-Wen Wei. Topological Charge and Black Hole Photon Spheres. *Phys. Rev. D*, 102(6):064039, 2020. [arXiv:2006.02112](#), [doi:10.1103/PhysRevD.102.064039](#).
- [29] Rajes Ghosh and Sudipta Sarkar. Light rings of stationary spacetimes. *Phys. Rev. D*, 104(4):044019, 2021. [arXiv:2107.07370](#), [doi:10.1103/PhysRevD.104.044019](#).
- [30] Chen-Kai Qiao and Ming Li. Geometric approach to circular photon orbits and black hole shadows. *Phys. Rev. D*, 106(2):L021501, 2022. [arXiv:2204.07297](#), [doi:10.1103/PhysRevD.106.L021501](#). III
- [31] Pedro V. P. Cunha, Emanuele Berti, and Carlos A. R. Herdeiro. Light-Ring Stability for Ultracompact Objects. *Phys. Rev. Lett.*, 119(25):251102, 2017. [arXiv:1708.04211](#), [doi:10.1103/PhysRevLett.119.251102](#). III
- [32] Guangzhou Guo, Peng Wang, Houwen Wu, and Haitang Yang. Quasinormal modes of black holes with multiple photon spheres. *JHEP*, 06:060, 2022. [arXiv:2112.14133](#), [doi:10.1007/JHEP06\(2022\)060](#). III A 1, V
- [33] Guangzhou Guo, Peng Wang, Houwen Wu, and Haitang Yang. Echoes from hairy black holes. *JHEP*, 06:073, 2022. [arXiv:2204.00982](#), [doi:10.1007/JHEP06\(2022\)073](#). III A 1
- [34] Tim Johannsen and Dimitrios Psaltis. A Metric for Rapidly Spinning Black Holes Suitable for Strong-Field Tests of the No-Hair Theorem. *Phys. Rev. D*, 83:124015, 2011. [arXiv:1105.3191](#), [doi:10.1103/PhysRevD.83.124015](#). III A 2
- [35] Nicolas Yunes and Leo C. Stein. Non-Spinning Black Holes in Alternative Theories of Gravity. *Phys. Rev. D*, 83:104002, 2011. [arXiv:1101.2921](#), [doi:10.1103/PhysRevD.83.104002](#). III A 2
- [36] Luciano Rezzolla and Alexander Zhidenko. New parametrization for spherically symmetric black holes in metric theories of gravity. *Phys. Rev. D*, 90(8):084009, 2014. [arXiv:1407.3086](#), [doi:10.1103/PhysRevD.90.084009](#). III A 3, III A 3
- [37] Prashant Kocherlakota and Luciano Rezzolla. Distinguishing gravitational and emission physics in black hole imaging: spherical symmetry. *Mon. Not. Roy. Astron. Soc.*, 513(1):1229–1243, 2022. [arXiv:2201.05641](#), [doi:10.1093/mnras/stac891](#).
- [38] Prashant Kocherlakota and Luciano Rezzolla. Comment on the Analytical Bounds in the Rezzolla-Zhidenko Parametrization. 6 2022. [arXiv:2206.03146](#). III A 3

- [39] R. A. Konoplya and A. Zhidenko. Analytical representation for metrics of scalarized Einstein-Maxwell black holes and their shadows. *Phys. Rev. D*, 100(4):044015, 2019. [arXiv:1907.05551](https://arxiv.org/abs/1907.05551), [doi:10.1103/PhysRevD.100.044015](https://doi.org/10.1103/PhysRevD.100.044015). III B 1
- [40] Peng Wang, Houwen Wu, and Haitang Yang. Scalarized Einstein-Born-Infeld black holes. *Phys. Rev. D*, 103(10):104012, 2021. [arXiv:2012.01066](https://arxiv.org/abs/2012.01066), [doi:10.1103/PhysRevD.103.104012](https://doi.org/10.1103/PhysRevD.103.104012).
- [41] Guangzhou Guo, Peng Wang, Houwen Wu, and Haitang Yang. Scalarized Einstein–Maxwell–scalar black holes in anti-de Sitter spacetime. *Eur. Phys. J. C*, 81(10):864, 2021. [arXiv:2102.04015](https://arxiv.org/abs/2102.04015), [doi:10.1140/epjc/s10052-021-09614-7](https://doi.org/10.1140/epjc/s10052-021-09614-7).
- [42] Guangzhou Guo, Peng Wang, Houwen Wu, and Haitang Yang. Thermodynamics and phase structure of an Einstein-Maxwell-scalar model in extended phase space. *Phys. Rev. D*, 105(6):064069, 2022. [arXiv:2107.04467](https://arxiv.org/abs/2107.04467), [doi:10.1103/PhysRevD.105.064069](https://doi.org/10.1103/PhysRevD.105.064069). III B 1
- [43] Vitor Cardoso, Kyriakos Destounis, Francisco Duque, Rodrigo Panosso Macedo, and Andrea Maselli. Black holes in galaxies: Environmental impact on gravitational-wave generation and propagation. *Phys. Rev. D*, 105(6):L061501, 2022. [arXiv:2109.00005](https://arxiv.org/abs/2109.00005), [doi:10.1103/PhysRevD.105.L061501](https://doi.org/10.1103/PhysRevD.105.L061501). III B 2, III B 2
- [44] Jorge Ovalle. Decoupling gravitational sources in general relativity: from perfect to anisotropic fluids. *Phys. Rev. D*, 95(10):104019, 2017. [arXiv:1704.05899](https://arxiv.org/abs/1704.05899), [doi:10.1103/PhysRevD.95.104019](https://doi.org/10.1103/PhysRevD.95.104019). III B 3
- [45] J. Ovalle. Decoupling gravitational sources in general relativity: The extended case. *Phys. Lett. B*, 788:213–218, 2019. [arXiv:1812.03000](https://arxiv.org/abs/1812.03000), [doi:10.1016/j.physletb.2018.11.029](https://doi.org/10.1016/j.physletb.2018.11.029).
- [46] J. Ovalle, R. Casadio, E. Contreras, and A. Sotomayor. Hairy black holes by gravitational decoupling. *Phys. Dark Univ.*, 31:100744, 2021. [arXiv:2006.06735](https://arxiv.org/abs/2006.06735), [doi:10.1016/j.dark.2020.100744](https://doi.org/10.1016/j.dark.2020.100744). III B 3
- [47] Harald H. Soleng. Charged black points in general relativity coupled to the logarithmic U(1) gauge theory. *Phys. Rev. D*, 52:6178–6181, 1995. [arXiv:hep-th/9509033](https://arxiv.org/abs/hep-th/9509033), [doi:10.1103/PhysRevD.52.6178](https://doi.org/10.1103/PhysRevD.52.6178). IV
- [48] Eloy Ayon-Beato and Alberto Garcia. Regular black hole in general relativity coupled to nonlinear electrodynamics. *Phys. Rev. Lett.*, 80:5056–5059, 1998. [arXiv:gr-qc/9911046](https://arxiv.org/abs/gr-qc/9911046), [doi:10.1103/PhysRevLett.80.5056](https://doi.org/10.1103/PhysRevLett.80.5056).
- [49] Hideki Maeda, Mokhtar Hassaine, and Cristian Martinez. Lovelock black holes with a nonlinear Maxwell field. *Phys. Rev. D*, 79:044012, 2009. [arXiv:0812.2038](https://arxiv.org/abs/0812.2038), [doi:10.1103/PhysRevD.79.044012](https://doi.org/10.1103/PhysRevD.79.044012).
- [50] Zhong-Ying Fan and Xiaobao Wang. Construction of Regular Black Holes in General Relativity. *Phys. Rev. D*, 94(12):124027, 2016. [arXiv:1610.02636](https://arxiv.org/abs/1610.02636), [doi:10.1103/PhysRevD.94.124027](https://doi.org/10.1103/PhysRevD.94.124027).
- [51] S.H. Hendi, B. Eslam Panah, S. Panahiyan, and A. Sheykhi. Dilatonic BTZ black holes with power-law field. *Phys. Lett. B*, 767:214–225, 2017. [arXiv:1703.03403](https://arxiv.org/abs/1703.03403), [doi:10.1016/j.physletb.2017.01.066](https://doi.org/10.1016/j.physletb.2017.01.066).
- [52] Jun Tao, Peng Wang, and Haitang Yang. Testing holographic conjectures of complexity with Born–Infeld black holes. *Eur. Phys. J. C*, 77(12):817, 2017. [arXiv:1703.06297](https://arxiv.org/abs/1703.06297), [doi:10.1140/epjc/s10052-017-5395-3](https://doi.org/10.1140/epjc/s10052-017-5395-3).
- [53] Peng Wang, Houwen Wu, and Haitang Yang. Thermodynamics of nonlinear electrodynamics black

- holes and the validity of weak cosmic censorship at charged particle absorption. *Eur. Phys. J. C*, 79(7):572, 2019. [doi:10.1140/epjc/s10052-019-7090-z](https://doi.org/10.1140/epjc/s10052-019-7090-z). IV
- [54] M. Novello, V. A. De Lorenci, J. M. Salim, and Renato Klippert. Geometrical aspects of light propagation in nonlinear electrodynamics. *Phys. Rev. D*, 61:045001, 2000. [arXiv:gr-qc/9911085](https://arxiv.org/abs/gr-qc/9911085), [doi:10.1103/PhysRevD.61.045001](https://doi.org/10.1103/PhysRevD.61.045001). IV, IV, IV
- [55] M. Born and L. Infeld. Foundations of the new field theory. *Proc. Roy. Soc. Lond. A*, 144(852):425–451, 1934. [doi:10.1098/rspa.1934.0059](https://doi.org/10.1098/rspa.1934.0059). IV B
- [56] Tanay Kr. Dey. Born-Infeld black holes in the presence of a cosmological constant. *Phys. Lett. B*, 595(1-4):484–490, 2004. [arXiv:hep-th/0406169](https://arxiv.org/abs/hep-th/0406169), [doi:10.1016/j.physletb.2004.06.047](https://doi.org/10.1016/j.physletb.2004.06.047). IV B
- [57] Rong-Gen Cai, Da-Wei Pang, and Anzhong Wang. Born-Infeld black holes in (A)dS spaces. *Phys. Rev. D*, 70:124034, 2004. [arXiv:hep-th/0410158](https://arxiv.org/abs/hep-th/0410158), [doi:10.1103/PhysRevD.70.124034](https://doi.org/10.1103/PhysRevD.70.124034). IV B
- [58] Aoyun He, Jun Tao, Peng Wang, Yadong Xue, and Ling kai Zhang. Effects of Born-Infeld electrodynamics on black hole shadows. *Eur. Phys. J. C*, 82(8):683, 2022. [arXiv:2205.12779](https://arxiv.org/abs/2205.12779), [doi:10.1140/epjc/s10052-022-10637-x](https://doi.org/10.1140/epjc/s10052-022-10637-x). IV B
- [59] Eloy Ayon-Beato and Alberto Garcia. The Bardeen model as a nonlinear magnetic monopole. *Phys. Lett. B*, 493:149–152, 2000. [arXiv:gr-qc/0009077](https://arxiv.org/abs/gr-qc/0009077), [doi:10.1016/S0370-2693\(00\)01125-4](https://doi.org/10.1016/S0370-2693(00)01125-4). IV C
- [60] The mathematica notebook is publicly available as ancillary files. V
- [61] Vitor Cardoso, Luís C. B. Crispino, Caio F. B. Macedo, Hirotada Okawa, and Paolo Pani. Light rings as observational evidence for event horizons: long-lived modes, ergoregions and nonlinear instabilities of ultracompact objects. *Phys. Rev. D*, 90(4):044069, 2014. [arXiv:1406.5510](https://arxiv.org/abs/1406.5510), [doi:10.1103/PhysRevD.90.044069](https://doi.org/10.1103/PhysRevD.90.044069). V
- [62] Pedro V. P. Cunha, Carlos Herdeiro, Eugen Radu, and Nicolas Sanchis-Gual. The fate of the light-ring instability. 7 2022. [arXiv:2207.13713](https://arxiv.org/abs/2207.13713). V